# Control of a hybrid helicopter with wings

de Wagter, Christophe; Smeur, Ewoud

**DOI**
10.1177/1756829317702674

**Publication date**
2017

**Document Version**
Final published version

**Published in**
International Journal of Micro Air Vehicles

Article

International Journal of Micro Air Vehicles

International Journal of Micro Air Vehicles
2017, Vol. 9(3) 209–217

DOI: 10.1177/1756829317702674
journals.sagepub.com/home/mav
SAGE

# Control of a hybrid helicopter with wings

**Christophe De Wagter and Ewoud JJ Smeur**

**Abstract**

This work investigates the design parameters and their consequences in the control of a helicopter rotor combined with a pair of fixed wings. This hybrid vehicle has a light and aerodynamically efficient rotor with a large range of pitch angles to enable both hover and forward flight. Because of the light stiff rotor and heavy wings, the hybrid vehicle exhibits couplings between the roll and pitch axes during hover flight. The rotor-wing interaction depends on a lot of parameters. In this article, we utilize a simplified theoretic model and simulations in order to gain insight in the effect of these parameters on the vehicle dynamics. Finally, a controller is designed that compensates undesired coupling between pitch and roll.

**Keywords**

Hybrid, micro air vehicle, rotor head, control, swash plate, model

Date received: 14 December 2016; accepted: 27 January 2017

## Introduction

Rotorcraft dynamics have been well studied for many years[1–4] with work ranging from rotorcraft modeling in Johnson[5] and Cai et al.,[6] rotorcraft simulation in Padfield,[7] over matching measurement data with models in Yamauchi et al.,[8] to the blade optimization in function of vibrations in Peters et al.[9] The design of controllers for conventional helicopters is well understood as shown in Shim et al.[10] and Gavrilets.[11]

For less conventional designs like hinge-less low inertia rotors or high inertia fuselages, the design choices and control problems are more complex. Ormiston[12] performed some studies into the fuselage-rotor interaction and fuselage ground interaction and has identified resonance problems.

On the scale of small unmanned helicopters, models were used in Caradonna and Tung[13] to identify which parameters affect the performance. Bernardini et al.[14] used a model to understand and reduce vibrations or noise. Recent work by Cai et al.[6] presents a comprehensive non-linear model of a miniature unmanned helicopter.

### *Heli-Wing hybrid*

The helicopter with wings concept is a hybrid UAV and has been introduced by De Wagter et al.[15] While the central part is using a standard rotor head, due to the lower blade weights and huge fuselage inertia, the properties identified by previous literature do not describe the characteristics of an efficient helicopter with wings.

When designing a complex hybrid vehicle, it is crucial to gain deeper insight into the different parameters that affect control and performance. Therefore, the subject of this article is the identification of the design parameters and control properties of a conventional cyclic and collective pitch controlled light rotor on top of a fixed wing shaped heavy fuselage. Figure 1 shows the vehicle in semi transitioned attitude. A schematic drawing of the hover and forward flight states is shown in Figure 2. The rotor allows the vehicle to hover while the wings and rotor design enable efficient fast forward flight.

The rotor blade design in the case of this vehicle is a compromise between efficient hover and efficient forward flight. This means the rotor is significantly different from rotors seen in conventional helicopters. It is relatively small, light, and stiff and it has a high lift coefficient. During forward flight, the *rpm* is reduced and pitch angle increased to generate propulsion efficiently. The large wings act as fuselage, and systems are

Micro Air Vehicle Laboratory, Delft University of Technology, Delft, The Netherlands

**Corresponding author:**
Christophe De Wagter, Micro Air Vehicle Laboratory, Delft University of Technology, Kluyverweg 1, Delft 2629HS, The Netherlands.
Email: c.dewagter@tudelft.nl

**Figure 1.** Novel hybrid Unmanned Air Vehicle featuring a cyclic controlled rotor with wing.

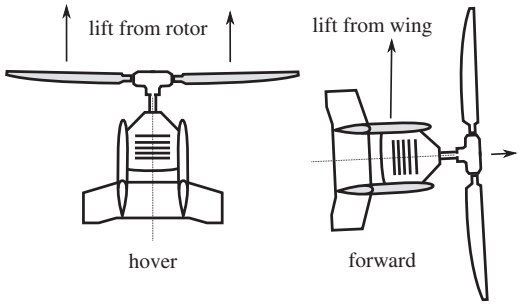


**Figure 2.** Hover and forward flight.

distributed over the entire wing, giving it a large moment of inertia.

These properties significantly affect the way the conventional helicopter rotor behaves during hover. On the other hand, during forward flight, the propulsion gyroscopic effect is much larger than usual, which also has an influence on the vehicle's dynamics.

In order to find an acceptable compromise between the dynamics in hover and forward flight, a mathematical model is created in the first section. In the next section, design parameters are varied. Following, the interaction between rotor and fuselage is investigated, and finally the model is used to gain insight in the flight test results of hovering flight.

## Rotor model

To explore the design options and their consequences, a helicopter model is derived mathematically.

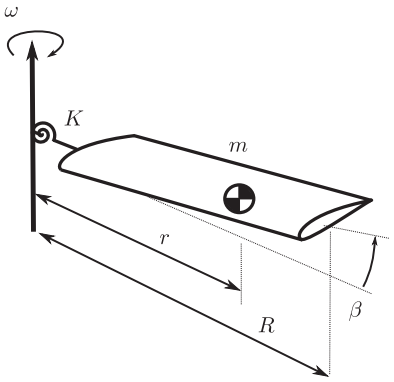


**Figure 3.** Simplified rigid rotor model.

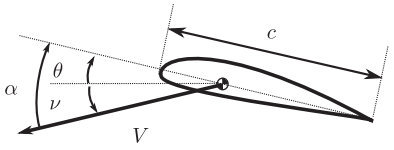


**Figure 4.** Angle of attack on a rotor section.

Figure 3 illustrates a basic rotor model similar to Bramwell et al.[4] The flapping angle $\beta$ is measured around the spring hinge $K$. The rotor radius is $R$ and it is spinning with a rate $\omega$. The inputs are deflections of the swash-plate around the body $x$ axis $\delta_x$ and $y$ axis $\delta_y$. A positive input $\delta_x$ increases the pitch of the blade as it passes over the $y$ axis.

A blade element and its corresponding angles are illustrated in Figure 4. The model neglects the lagging angle of the rotor blade. The velocity $V_x$ of the blade element then becomes $\omega r$ while the vertical speed of the blade element $V_y$ is a function of the derivative of the flapping rate $\dot{\beta}r$. The path angle $\nu$ is the arc tangent of $V_x$ and $V_y$ while $\theta$ is the feathering angle of the blade and is set with collective and cyclic pitch commands. The velocity of a blade element then is:

$$\bar{V} = \begin{pmatrix} V_x \\ V_y \end{pmatrix} = \begin{pmatrix} \omega r \\ \dot{\beta} r \end{pmatrix} \tag{1}$$

Since we are mainly interested in the lateral control properties, we will neglect collective pitch, meaning that there will be no induced velocity $v_i$ and the angle of attack of a blade element is $\alpha = \theta - \nu$, and for small angles $\nu = \dot{\beta}/\omega$. The lift on a blade element becomes:

$$\delta L = \frac{\rho}{2}(\omega r)^2 C_L(\alpha) \cdot c \delta r \tag{2}$$

in which the lift coefficient $C_L(\alpha)$ during hover condition can be linearized to $c_{l_\alpha}\alpha$ and $\rho$ is the air density.

$c$, $\theta$, $\alpha$, and $R$ are defined in Figures 3 and 4. The *Lock Number* $\gamma = \rho c_{l_\alpha} c R^4 / I$ is substituted with $I$ being the rotational inertia of the rotor[4]

$$\delta L = \gamma \frac{\omega^2 I}{R^4} \left( \theta - \frac{\dot{\beta}}{\omega} \right) \cdot \frac{1}{2} r^2 \cdot \delta r \tag{3}$$

First the moments created by a blade element are integrated. The centrifugal force $r\cos(\beta) \cdot \omega^2 \cdot \delta m$ and the aerodynamic force $\delta L$ on a blade element together with the mass $\delta m$ of the blade element yield the following blade moment at the hinge:

$$\begin{aligned} M_{blade} = & \int r \cdot \delta L \\ & - \int \cdot \omega^2 \cdot r\cos(\beta) \cdot r\sin(\beta) \cdot \delta m \\ & - \int r \cdot \delta m \end{aligned} \tag{4}$$

where $\delta L$ is expressed in function of $\delta r$ in equation (3). $\delta m$ can be expressed in function of a length unit $\delta r$ using the rotor density $\rho_{blade}$ and its cross section $S_{cross\_section}$. The equation can then be integrated over the length of the rotor blade $R$.

Then the hinge spring moment $K \cdot \beta$ is added to the blade moment $M_{blade}$. To obtain the blade dynamics $\ddot{\beta}$, the sum of moments is divided by the blade rotational inertia $I = \int r^2 \delta m$.

When linearizing equation (4), filling the lift force from equation (3), neglecting the very small contribution of gravity on the blade dynamics and integrating over a uniform rotor, the differential equation[4] for flapping around a fixed hinge is obtained:

$$\ddot{\beta} + \frac{\gamma}{8}\omega\dot{\beta} + \left( \omega^2 + \frac{K}{I} \right) \beta = \frac{\gamma}{8}\omega^2\theta \tag{5}$$

Equation (5) relates the inertia of the rotor, the aerodynamic damping, and the centrifugal and spring forces to the excitation. The three main design parameters are shown to be the rotor rpm $\omega$, the spring stiffness $K$, and the *Lock Number* $\gamma$, which relates the rotor lift properties to its mass properties.

In simulation, the rotor is defined as a finite number of sections and integral in equation (4) is replaced by a summation over all segments.

The excitation using feathering angle $\theta$ is periodic and a function of the control inputs $\delta_x$ and $\delta_y$

$$\theta = \delta_y \sin(\omega t) + \delta_x \cos(\omega t) \tag{6}$$

## Design variation

The derived model is analyzed in simulation. To gain insight into the design choices, several variables in the model that can be tuned in real life are varied over a range.

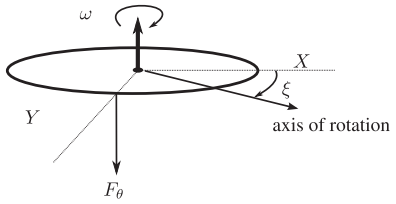


**Figure 5.** Blade dynamics based on cyclic deflection with zero spring stiffness $K$.

**Table 1.** Blade parameters.

| Variable | Value | Unit |
|---|---|---|
| $R$ | 51 | cm |
| $r_{c.g.}$ | 30 | cm |
| $m$ | 55 | g |
| $c_{tip}$ | 3.0 | cm |
| $c_{root}$ | 5.7 | cm |
| $c_{l_\alpha}$ | $2\pi$ | cm |
| $K$ | 88 | Nm/rad |

**Table 2.** Fuselage parameters.

| Variable | Value | Unit |
|---|---|---|
| $x_{c.g._{wing}}$ | .8 | m |
| $y_{c.g._{wing}}$ | .12 | m |
| $m_{wing}$ | 0.95 | kg |
| $m_{total}$ | 3.9 | kg |

**Table 3.** Central rotor block spring mounts.

| Variable | Value | Unit |
|---|---|---|
| $m_{weight}$ | 730 | g |
| $r_{weight}$ | 41 | cm |
| $r_{deflect}$ | 41 | cm |
| $\Delta_{z_{tip}}$ | 17 | mm |

### Hinged rotor

Figure 5 shows the results for a rotor with $K = 0$. Parameters for the model can be found in Tables 1 to 3. A deflection $\delta_y$ of 4° is applied. After a few rotations,[a] the rotor plane is tilted.

The deflection $\beta$ has a phase lag of 90° with the perturbation $\theta$ as is expected in gyroscopes. $\xi$ (see Figure 6) is equal to 90°. A positive cyclic deflection in pitch decreases the feathering angle $\theta$ whenever the rotor blade is at the right side of the vehicle with a $\omega$

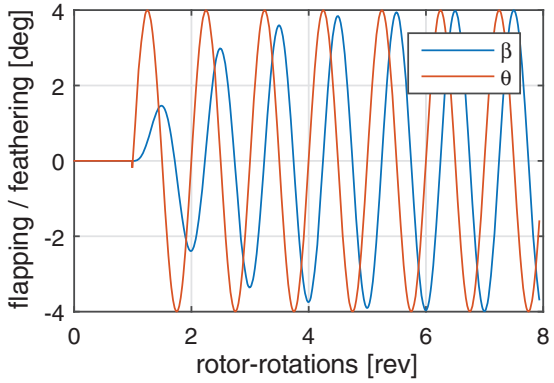


**Figure 6.** Applied force $F_\theta$ on a spinning rotor and corresponding axis of rotation at angle $\xi$. For non spinning bodies, $\xi$ is zero as a moment in the $x$ axis will produce a rotation in the $x$ axis. For pure gyroscopes $\xi$ is 90°.

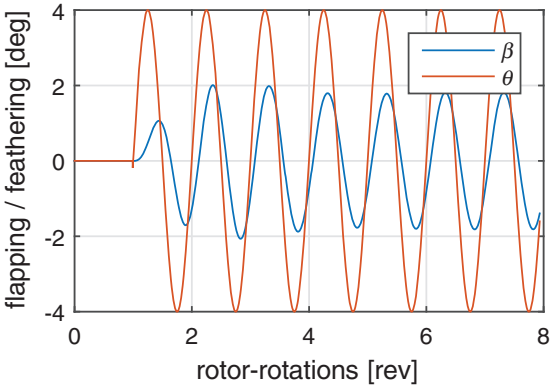


**Figure 7.** Blade dynamics based on cyclic deflection with significant spring stiffness $K$.

clockwise spinning rotor, to yield a rotor-plane inclination backward.

### *Stiff rotor*

When the stiffness of the spring $K$ is increased, the dynamics of the rotor are significantly affected. Not only is the deflection $\beta$ reduced, but also the direction of maximal flapping—in other words the rotor plane rotation—is affected.

Figure 7 shows the results for a rotor system with a stiff spring (high $K$). In this case, the angle $\xi$, or in other words, the phase difference between $\theta$ and $\beta$, is reduced from 90° to below 30° for a spring $K$, which reduces the flapping angle $\beta$ roughly by half.

### *Design parameters*

The theoretic model gives great insights on how the real rotor head and rotor can be tuned or modified. Equation (5) shows that the dynamics of the rotor are affected by the rotor rotation rate $\omega$, *Lock Number* $\gamma$, and spring stiffness with respect to rotor inertia $K/I$.

Practically, however, for a given amount of lift and given size, the rotation rate is quite determined and the *Lock Number* $\gamma$ can only be altered easily by changing the rotor weight. The rotor weight will mainly influence the speed of the response. The spring stiffness $K$ can be changed easily and affects the dynamics of the rotor significantly.

## Rotor head and fuselage

### *Rotor head model*

Since the previous sections have shown the importance of the hinge spring, the model of the actual rotor is investigated further. Figure 8 shows a cross section of

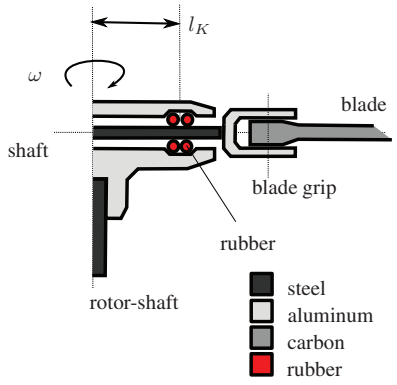


**Figure 8.** Actual rotor hub simplified schematics.

the helicopter rotor head used in the platform from Figure 1. It consists of an aluminum head block on a main rotor shaft. The shaft holding both blades is only connected to the hub via rubber o-rings. A close up can be seen in Figure 9.

Modeling the bending of all parts of the rotor is complex. The exact bending of the feathering shaft, the blade grips, and the blade itself contain a large number of parameters. Modeling how the force is transferred from the rotor system to the main rotor shaft is simplified by modeling only the rubber o-rings with linear stiffness $K_{o-ring}$ and their location $l_{o-ring}$ as illustrated in Figure 10. For one blade, the moment from the rotor on the rotor shaft becomes:

$$M_{rotor-shaft} = \Delta z_{o-ring} \cdot K_{o-ring} \cdot l_{o-ring} \tag{7}$$

Equation (5) is using a torsional spring constant $K$. The relation between the linear spring constant $K_{o-ring}$ and torsional spring constant $K$ is given by:

$$K = K_{o-ring} \cdot l_{o-ring}^2 \tag{8}$$

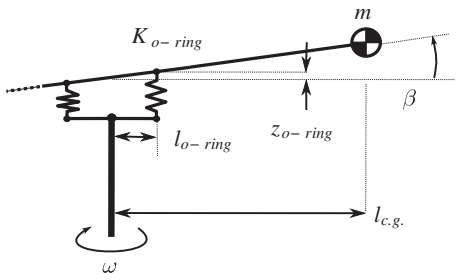


**Figure 9.** Close up of the rotor head of the hybrid winged helicopter vehicle. The swash-plate has 3 servos at 120° from each other. Collective pitch has much greater reach than conventional helicopters and the blades have more twist to allow efficient forward flight.

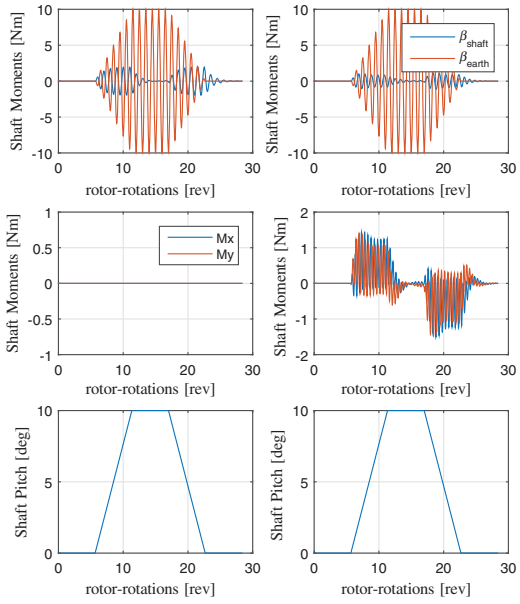


**Figure 10.** Simplified rotor hub.

## Constrained rotor-shaft motion

When the rotor shaft is rotated in pitch or roll to simulate a fuselage change in attitude, the rotor plane is following the fuselage motion. Figure 11 depicts the simulation results of a 10° pitch up of the fuselage and main rotor shaft in the case of a pure hinged rotor with $K = 0$ and in the case of a bending rotor with $K$ non-zero.

In the case of a fully hinged rotor, the rotor disc still tracks the motion of the rotor-shaft, as the feathering angle of the blade remains parallel to the rotor shaft through the swash-plate dynamics. When neglecting the blade grip push-rods and swash-plate forces, the moment from rotor to rotor shaft is zero.

On the other hand, whenever a moment can be transferred from the rotor to the rotor-shaft, it can be seen that the relative blade flapping angle $\beta_{shaft}$ creates

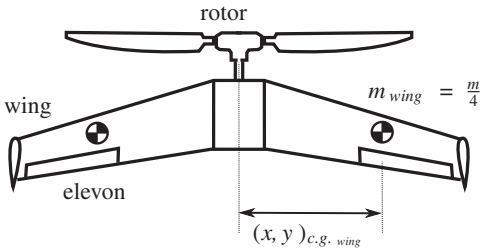


**Figure 11.** Rotor dynamics in function of fuselage imposed motion. Left $K = 0$, right $K \neq 0$.

moments $M_x$ and $M_y$ with a frequency of $2\omega$, or two times the rotor frequency.

It is interesting to note that a pure imposed pitch motion will generate moments in both $M_x$ and $M_y$ directions. The fuselage applies a moment to the rotor to make it pitch up, but the gyroscopic reaction of the rotor on that pitching motion is a rolling motion. This yields a roll moment from the rotor on the fuselage in return.

This is of particular importance in the case of a partially constrained fuselage. For instance, upon landing of the vehicle from Figure 1 with a roll angle, one tip will touch the ground first, yielding a constrained roll rate imposed on the rotor. As shown in Figure 11, this results in significant pitch moments imposed back from the rotor on the fuselage. This can lead to undesired pitch motions caused by imposed roll motions.

Similarly, in forward flight, a pitching moment from the fixed wing and its elevons will cause an undesired yawing moment from the rotor back on the fuselage.

## Free fuselage dynamics

To simulate the free fuselage dynamics, the fuselage is modeled as four point loads of a quarter of the total mass, as depicted in Figure 12. The fuselage is symmetric around the $x$ and $y$ axes, but the dimensions are not equal.

The distance from the vehicle center of gravity to each modeled point load $m_{wing}$ in the $x$ direction is $l_x$ and in the $y$ direction is $l_y$.

$$I_{xx} = \frac{m}{4} \cdot x_{c.g._{wing}} \tag{9}$$

$$I_{yy} = \frac{m}{4} \cdot y_{c.g._{wing}} \tag{10}$$

Assuming no aerodynamic forces on the wing during hover, no yaw rate, and small angles, the fuselage rates

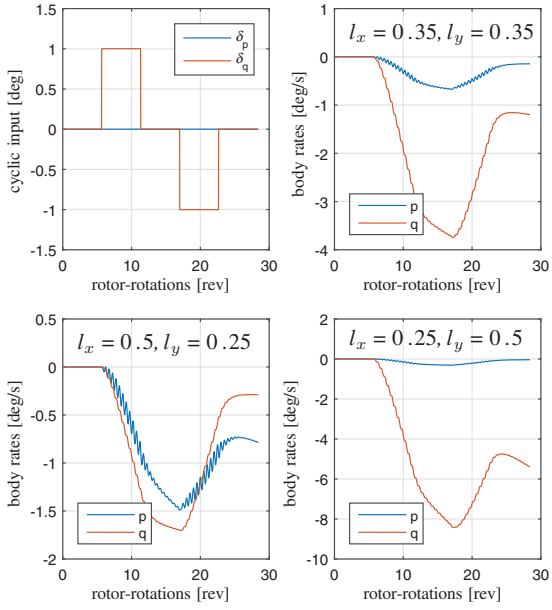


**Figure 12.** Body model.

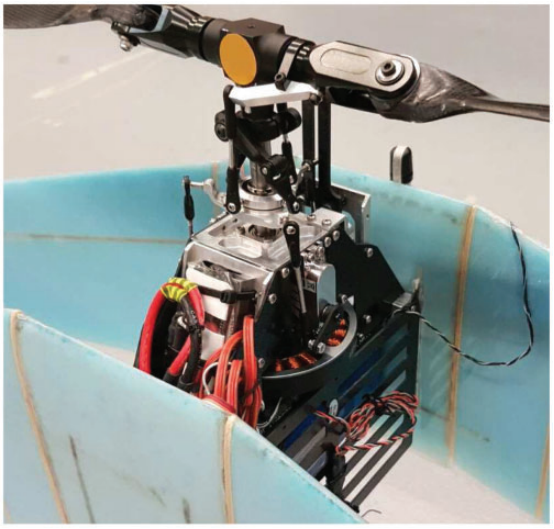

**Figure 13.** The influence of fuselage inertia on a free body. Three simulations of an identical rotor with identical non-zero stiffness and different inertia distribution of the fuselage.

are obtained through integration of the rotor shaft moments.

$$p_{fuselage} = \int_0^t \frac{M_x}{I_{xx}} \mathrm{d}t \tag{11}$$

$$q_{fuselage} = \int_0^t \frac{M_y}{I_{yy}} \mathrm{d}t \tag{12}$$

Using this simple vehicle model, the interaction between the rotor and the fuselage can be simulated. In Figure 13, three of these simulations are shown, for different values of $l_x$ and $l_y$. For all three simulations, the same inputs are applied, shown in the top left figure. Clearly, the distribution of fuselage inertia over the $X$ and $Y$ axes has a big influence on the way the vehicle reacts to inputs.

## Control considerations

The insights from the derived models were applied to the control of the hybrid rotor-wing vehicle depicted in Figure 1. It has very light, stiff, and relatively small carbon-fiber rotor blades, mounted on a stiff conventional Logo-480 rotor head with modified blade grips and doubled pitch range. The rotor blade airfoils are highly cambered to obtain high lift coefficients. Parameters of the vehicle are given in Tables 1 to 3 and in De Wagter et al.[15] The wing-shaped fuselage is very wide and heavy. This combination is not behaving like a conventional helicopter anymore.

To obtain real flight tests data, the vehicle was equipped with an autopilot with a simple low gain

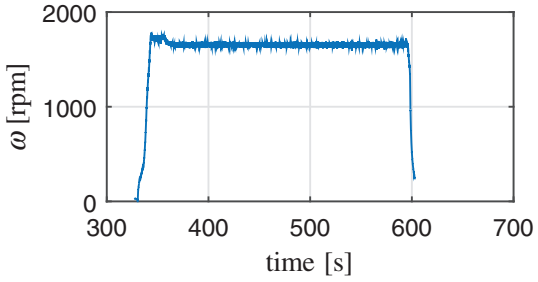


**Figure 14.** Test flight RPM.

rate controller. A governor was also programmed to yield a constant rpm and hereby remove extra variables from the problem. Figure 14 shows the rpm is kept constant as soon as the vehicle takes off. The flight controller used is the paparazzi autopilot project as described in literature.[16–18]

In steady conditions, the vehicle can just be kept airborne with a simple low gain proportional controller that controls the vehicle's angular rates. The output of this controller is cyclic commands, which are mapped to the three servos that control the swash-plate. The feedback was initially done with a 90° offset (see Figure 6), such that roll feedback was applied to $\delta_x$ and pitch feedback to $\delta_y$. $\delta_x$ produces a moment in the pitch axis and $\delta_y$ produces a moment in the roll axis. Due to gyroscopic precession, this then produces an angular rate in the desired axis. This method of control is very common for helicopters.[4]

For the vehicle in question, this controller did not provide control without couplings. Inputs of the pilot

resulted in rates in a different axis than intended and on top of that a transient "wobble," where the vehicle oscillates in both pitch and roll with a 90° phase difference. Using onboard logging on an SD card, all turn rates and control deflections were logged.

These data were used to model the angular acceleration in pitch and roll in function of the inputs $\delta_x$ and $\delta_y$, the rates in roll and pitch and an offset $O = 1$. The model is shown in equations (13) and (14), where $f_p$ and $f_q$ are linear functions of the parameters.

$$\dot{p} = f_p(O, \delta_x, \delta_y, p, q) \tag{13}$$

$$\dot{q} = f_q(O, \delta_x, \delta_y, p, q) \tag{14}$$

From the first data-set, it was discovered that the control mapping was incorrect, as $\delta_x$ and $\delta_y$ both caused a roll as well as a pitch rate acceleration. This was expected to cause some of the problems, which is why a second test flight was conducted using the corrected control mapping.

Figure 15 shows the angular acceleration in roll and pitch along with the best fit of $f_p()$ and $f_q()$ for this second flight. All signals were filtered with a second-order filter with a cutoff frequency of 15 rad/s, such that all signals have the same delay.[19] The plot shows a 20° step in roll. From the figure, it can be seen that the model fit is very accurate for this part of the flight. Figure 16 shows the pitch and roll rates for this flight. From this figure, it is clear that that the transient wobble was still present. This is attributed to the effect of the rate on angular acceleration in the other axis. The coefficients that were found using the data shown in Figure 15 are shown in Table 4.

Note the coefficients for $C_p$ and $C_q$. They state that a roll rate causes a pitch acceleration and vice verse. This might well explain the observed wobble. Therefore, in order to remove the wobble, the angular acceleration due to the rates needs to be canceled by a control input. The linear controller is revised to:

$$\begin{bmatrix} \delta_x \\ \delta_y \end{bmatrix} = G^{-1} \begin{bmatrix} K_p p_{err} + q C_{q_{\dot{p}}} K_c \\ K_q q_{err} + p C_{p_{\dot{q}}} K_c \end{bmatrix} \tag{15}$$

where $p_{err}$ and $q_{err}$ are the difference between the pilot command and the actual rates of the vehicle, and

$$G = \begin{bmatrix} C_{\delta_{x_{\dot{p}}}} & C_{\delta_{y_{\dot{p}}}} \\ C_{\delta_{x_{\dot{q}}}} & C_{\delta_{y_{\dot{q}}}} \end{bmatrix} \tag{16}$$

And $K_c$ is a value between 0 and 1. $K_c$ was introduced in order to gradually enable the compensation of angular acceleration due to rates. Test flights showed

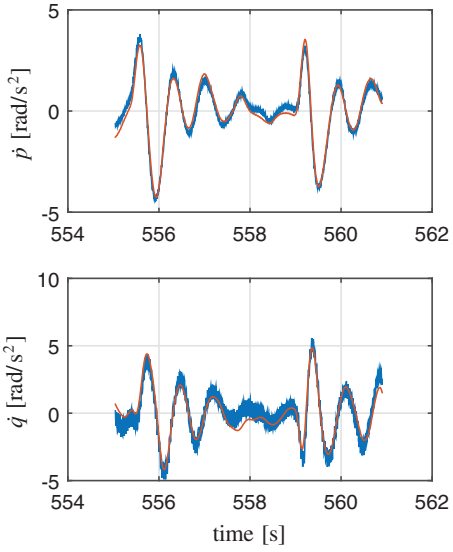


**Figure 15.** Fitting control inputs and body rates to body accelerations. In blue, the filtered angular acceleration and in red the best model fit.

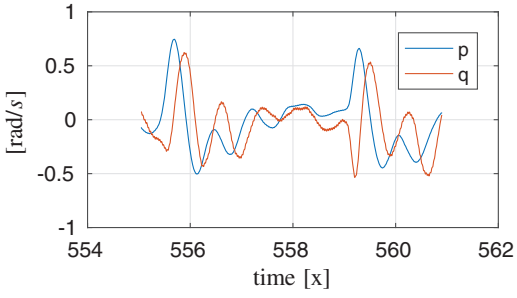


**Figure 16.** Flight with $K_c = 0$.

**Table 4.** Identified parameters.

| Coefficient | $f_p$ | $f_q$ |
|---|---|---|
| $C_O$ | −2.4661 | −2.8847 |
| $C_{\delta_x}$ | 0.0032 | −0.0044 |
| $C_{\delta_y}$ | 0.0011 | 0.0073 |
| $C_p$ | −0.5703 | 7.4479 |
| $C_q$ | −3.4308 | −3.4487 |

that a value of 0.5 gives better results than a value of 1. This may be caused by actuator dynamics, as a control moment can not be instantly generated when a rate is measured. More research is necessary to better explain why $K_c = 1$ still gives a wobble.

Figure 17 shows the measured angular rates of the vehicle during some pitch maneuvers in the first part of the flight ($t < 598$ s) and some roll maneuvers in the

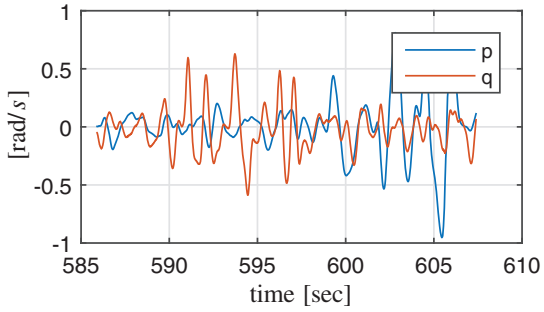


**Figure 17.** Flight with $K_c = 0.5$.

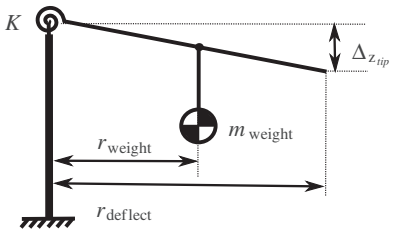


**Figure 18.** To measure the stiffness of the hinge springs and blade of the real aircraft, a measurement setup was created. A constant weight was added to the blade at a given distance and the resulting deflection was measured.

second part of the flight. The rates were filtered with a second-order filter with a cutoff frequency of 25 rad/s. From this figure, it can be seen that no wobble is present, and the motion in roll and pitch is uncoupled. Compare this to Figure 16, where $K_c = 0$ results in clear coupling between roll and pitch.

## Conclusion

When designing hybrids between conventional cyclic controlled helicopters and fixed wings, it is crucial to understand the interactions between rotor and wing in order to optimize the design. Although a simulation model can not provide direct control parameters, it can help understand the variables affecting performance and control.

*Lock Number* was shown to influence the response speed of the rotor while rotor hinge spring stiffness was shown to influence the amplitude of the rotor rotation and even direction of the control effectiveness. Compensation for actual control effectiveness was needed in the controller to obtain correct steering and feedback.

Non-homogeneous inertia of the fuselage and fuselage-rotor interactions add non-symmetrical coupling between the pitch and roll axes. Compensation for gyroscopic effects was needed in the controller to remove this coupling.

In future research, we want to identify more of the parameters discussed in the theory section of the article, in order to better predict the response of the vehicle to inputs. This information is vital in improving the performance of the current controller. Also, we want to investigate how the helicopter dynamics influence the dynamics in forward flight.

## Acknowledgements

We thank the sponsors of the TU-Delft Outback Medical Challenge 2016 Entry to have made this research possible. Moreover, we thank all members of the team for their great efforts in turning this project into a success. More information on the platform and the team can be found at http://www.delftacopter.nl

## Declaration of conflicting interests

The author(s) declared no potential conflicts of interest with respect to the research, authorship, and/or publication of this article.

## Funding

The author(s) received no financial support for the research, authorship, and/or publication of this article.

## Supplemental material

Parameters of the model are supplied below: To assess the stiffness of the central rotor block rubbers, a setup was created using a dummy weight to measure the increase in deflection as shown in Figure 18 with parameters from Table 3.

## Note

a. The number of rotations depends on the *Lock Number* $\gamma$ or in other words the damping to weight ratio.

## References

1. Stepniewski WZ and Keys C. *Rotary-wing aerodynamics*. Massachusetts: Courier Corporation, 1979.
2. Prouty RW. *Helicopter performance, stability, and control*. Melbourne, FL: Krieger Publishing Company, 1995.
3. Wagtendonk WJ. *Principles of helicopter flight*. Oxford, United Kingdom: Aviation Supplies & Academics Inc, 1996.
4. Bramwell AR, Balmford D and Done G. *Bramwell's helicopter dynamics*. Butterworth-Heinemann, 2001.
5. Johnson W. A comprehensive analytical model of rotorcraft aerodynamics and dynamics. Part 1. Analysis development. Technical Report, NASA Ames Research Center, DTIC Document, 1980.
6. Cai G, Chen BM, Lee TH, et al. Comprehensive nonlinear modeling of a miniature unmanned helicopter. *J Am Helicopter Soc* 2012; 57: 1–13.
7. Padfield GD. *Helicopter flight dynamics*. Hoboken, New Jersey, United States: John Wiley & Sons, 2008.
8. Yamauchi GK, Heffernan RM and Gaubert M. Correlation of sa349/2 helicopter flight test data with a

comprehensive rotorcraft model. *J Am Helicopter Soc* 1988; 33: 31–42.
9. Peters DA, Ko T, Korn A, et al. Design of helicopter rotor blades for desired placement of natural frequencies. In: *39th Annual forum American helicopter society*, St. Louis, Missouri, 1983, pp.674–689.
10. Shim H, Koo TJ, Hoffmann F, et al. A comprehensive study of control design for an autonomous helicopter. In: *Proceedings of 37th IEEE conference on decision and control*, Citeseer, 1998, pp.1–6.
11. Gavrilets V. Dynamic model for a miniature aerobatic helicopter. In: Valavanis K and Vachtsevanos GJ (eds) *Handbook of unmanned aerial vehicles*. Netherlands, Springer, 2015, pp. 279–306.
12. Ormiston RA. Rotor-fuselage dynamics of helicopter air and ground resonance. *J Am Helicopter Soc* 1991; 36: 3–20.
13. Caradonna F and Tung C. Experimental and analytical studies of a model helicopter rotor in hover. In: *European rotorcraft and powered lift aircraft forum*, Garmisch-Partenkirchen, Germany, 1981, pp.1–58.
14. Bernardini G, Piccione E, Anobile A, et al. Optimal design and acoustic assessment of low-vibration rotor blades. *Int J Rotat Mach*, Cairo 2016; 1–17.
15. De Wagter C, Ruijsink R, Smeur E, et al. Design, control and visual navigation of the delftacopter. 2017.
16. Brisset P, Drouin A, Gorraz M, et al. The paparazzi solution. In: *MAV 2006, 2nd US-European competition and workshop on micro air vehicles*, Sandestin, United States, 2006.
17. Gati B. Open source autopilot for academic research-the paparazzi system. In: *IEEE American control conference (ACC)*, Washington, DC, 2013, pp.1478–1481.
18. Hattenberger G, Bronz M and Gorraz M. Using the paparazzi UAV system for scientific research. In: *IMAV 2014, International micro air vehicle conference and competition*, Delft, The Netherlands, 2014, pp.247.
19. Smeur EJJ, Chu QP and de Croon GCHE. Adaptive incremental nonlinear dynamic inversion for attitude control of micro aerial vehicles. *J Guid Control Dyn* 2016; 39: 450–461.